Title

The Case for Combining a Large Low-Band Very High Frequency Transmitter With Multiple Receiving Arrays for Geospace Research: A Geospace Radar

Journal

Radio Science, 54(7)

ISSN

0048-6604

Authors

Hysell, DL
Chau, JL
Coles, WA
et al.

Publication Date

2019-07-01

DOI

10.1029/2018rs006688

Peer reviewed

Radio Science, Volume ???, Number , Pages 1–51,

The case for combining a large low-band VHF transmitter with multiple receiving arrays for geospace research: A Geospace Radar

D. L. Hysell[1], J. L. Chau[2], W. A. Coles[3], M. A. Milla[4], K. Obenberger[5], and J. Vierinen[6]

[1]Earth and Atmospheric Sciences, Cornell University, Ithaca, NY, USA

[2]Leibniz-Institute for Atmospheric Physics at the University of Rostock, Germany

[3]Electrical and Computer Engineering, U.C. San Diego

[4]Jicamarca Radio Observatory, Institute Geofisico del Peru

[5]Space Vehicles Directorate, Air Force Research Laboratory

[6]University of Tromso

Key Points.

1. A radar capable of probing a wide swath of Geospace could be assembled from a HPLA transmitter and a number of radio-array receivers.
2. Applications for such a geospace radar include MST, meteor, ionospheric, plasmaspheric, planetary, and solar research.
3. A geospace radar would promote discovery research and support space-weather applications.

We argue that combining a high-power, large-aperture (HPLA) radar transmitter with several large-aperture receiving arrays to make a geospace radar - a radar capable of probing near-earth space from the upper troposphere through to the solar corona - would transform geospace research. We review the emergence of incoherent scatter radar (ISR) in the 1960s as an agent which unified early, pioneering research in geospace in a common theoretical, experimental, and instrumental framework, and we suggest that a geospace radar would have a similar effect on future developments in space-weather research. **We then discuss recent developments in radio-array technology that could be exploited in the development of a geospace radar with new or substantially improved capabilities compared to the radars in use presently. A number of applications for a geospace radar with the new and improved capabilities** are reviewed including studies of meteor echoes, mesospheric and stratospheric turbulence, ionospheric flows, plasmaspheric and ionospheric irregularities, and reflection from the solar corona and coronal mass ejections (CMEs). We conclude with a summary of technical requirements.

1. Introduction and motivation

The object of geospace science is to explore and understand humanity's place in the solar system and the effects of variations in space on natural and technological systems. This encompasses studies of processes in regions ranging from the surface of the Sun through the interplanetary medium to the magnetosphere, radiation belts, plasmasphere, ionosphere, and neutral atmosphere enveloping the Earth. Some of these processes are detrimental to life and society and constitute space weather. The enormous scope of the problem and the breadth of its impacts demand a comprehensive, integrated response from multiple components of the scientific community working with a range of ground- and space-based instruments, the agencies that support them, and the countries in which they operate.

Similar comments would have been applicable at the start of the space age before the fundamentals of plasma physics, in space and in the laboratory, were firmly established. Scientists with a range of backgrounds struggled to understand the first observations of the ionosphere from early spacecraft and from radio and radar apparatus designed for other purposes in some instances, using different approaches and formalisms. A landmark event in the history of space physics was the development in the 1960s of a theory to explain ionospheric scattering of signals transmitted from high-power, large-aperture (HPLA) radars. What emerged, so-called "incoherent scatter theory," remains one of the most successful applications of linear plasma theory to a complicated natural phenomenon and a textbook example of how theory and technology can develop rapidly together. The legacy of the era is a world-wide network of Incoherent Scatter Radars (ISRs) that remains the source

of the most incisive and least ambiguous measurements of ionospheric plasmas available through remote sensing. Such radars are the centerpieces of the existing upper-atmospheric facilities and are complemented by radio as well as optical ground-based instruments. The upper-atmospheric facilities are well coordinated in the way they acquire, disseminate, and interpret their observations.

While the last half century has seen tremendous advances in radio technology, signal processing, and space-plasma theory, the ISRs function as much as they did in the early days of development. They are configured mainly for monostatic operation, utilizing large antennas or antenna arrays for transmission and reception. Beam steering, mechanical or electronic, remains the paradigm for surveying large volumes. The radars operate at high peak-power levels with relatively small duty cycles. Range resolution is enhanced mainly through pulse coding and pulse compression. Radar frequencies have mainly been chosen in the UHF band **for reasons having to do mainly with sky noise and licensing requirements.** Most of the ISRs concentrate their operating hours into specialized campaigns with durations of a few days or weeks with low-power survey modes filling the gaps. **These choices are rooted in history, including funding history and trends,** but are no longer especially well suited for either scientific discovery or space-weather surveillance.

In this paper, we explore the outlines of the next generation of HPLA radars for geospace research. The objective is to expand the coverage of the current radars to encompass a larger segment of geospace. The central concept combines a main radio array for transmission with multiple, higher-resolution arrays for reception in the low VHF band, bridging contemporary experimental principles from aeronomy and astronomy. The paper presents

a description of the current state of affairs, a discussion of the new capabilities modern radio arrays could provide, and a review of a few possible applications in geospace research. Underlying the discussion is the premise that a geospace radar would serve the same integrating role in the international space-physics community as the original ISRs that came before them.

2. Conventional high-power, large-aperture radars

Starting with Arecibo in Puerto Rico and Jicamarca in Peru, the upper-atmospheric facilities were established to provide ground-based remote-sensing of near-Earth space to complement observations coming from early spacecraft. The upper-atmospheric facilities were built around pulsed HPLA radars to exploit the principle of incoherent scatter. Incoherent scatter is modified Thompson scatter from fluctuations in free electron density in a plasma. The relationship between the spectra measured by the radar and the state variables in the ionosphere is given by incoherent scatter theory [*Salpeter*, 1960; *Fejer*, 1960; *Dougherty and Farley*, 1960; *Farley et al.*, 1961; *Fejer*, 1961; *Hagfors*, 1961; *Salpeter*, 1961; *Rosenbluth and Rostocker*, 1962; *Dougherty and Farley*, 1963; *Perkins et al.*, 1965; *Woodman*, 1967]. In principle, incoherent scatter can be used to measure electron number density, electron and ion temperature, ion composition, line-of-sight drifts, and collision frequencies. The energetic electron population can also be inferred from the measurements. Incoherent scatter theory becomes complicated in certain limits, notably for incidence angles close to perpendicular to the geomagnetic field. Some aspects of the theory, including the effects of Coulomb collisions on the spectra, are still topics of research and

further development [*Kudeki and Milla*, 2011; *Milla and Kudeki*, 2011]. Incoherent scatter is nonetheless the most direct and incisive technique we have for ionospheric remote sensing. Radars capable of incoherent scatter observations can presently be found in the United States and Canada, Peru, Scandinavia, Russia, Japan, and China. Other dual-use radars can be used for incoherent scatter such as the ALTAIR radar in the Kwajalein Atoll.

The upper-atmospheric facilities measure the most important state parameters in ionospheric plasmas. Neutral parameters, including temperatures and winds, are not observed directly but can be inferred from the plasma measurements (e.g. *Hysell et al.* [2014]). Higher-level ionospheric processes including chemistry, energetics, and transport can then be inferred from the state parameters through the application of conservation laws rooted in plasma kinetic or fluid theory. Nowadays, the conservation laws are typically encoded in computer models and simulations. Data from the upper-atmospheric facilities are either used for consistency checks for the models and simulations or incorporated directly through data assimilation. Data assimilation can be applied to very low-level radar data products, for example the spectra or autocorrelation functions of the signals themselves, avoiding some of the distortions inherent in estimating higher-level data products directly.

The sensitivity of an ISR is partly governed by its figure of merit, f, the product of the transmitter average power in Watts and the effective antenna aperture in square meters divided by the product of the sky noise temperature in Kelvin degrees and the receiver bandwidth in Hz:

$$f = \frac{PA}{BT} \tag{1}$$

The signal-to-noise ratio of a given experiment will be proportional to this figure [*Beynon and Williams*, 1978] Sensitivity also depends on other experimental characteristics, including the sampling cadence (which can be enhanced by exploiting frequency or polarization diversity) and the signal-processing strategy, and so the figure of merit is not a comprehensive measure of ISR preformance. Another useful measure is the speed of an experiment which quantifies the time required to achiave measuremens with a given statistical accuracy [*Lehtinen*, 1986]. The figure of merit nonetheless is a useful too for comparing and designing HPLA radars.

Arecibo, which has the highest figure of merit of any of the ISRs, operates in the UHF band near a minimum in the sky noise temperature. Jicamarca, meanwhile, operates at 50 MHz band where the sky noise temperature is two orders of magnitude greater (although the bandwidth required is also an order of magnitude smaller). The low frequency is disadvantageous from the point of view of the figure of merit but advantageous in a number of important ways. The figure of merit is, in fact, a limited metric which does not capture important tradeoffs involving the radar frequency, the characteristics of transmit and receive antennas, which could be different, or the characteristics of the emission and the way the signals are processed.

An advantage of VHF, for example, is improved immunity from finite Debye-length effects. The bandwidth of the ion line, the dominant incoherent scatter feature (at angles away from the perpendicular to the geomagnetic field direction), is determined by the ion rather than the electron thermal speed, but only if the the radar wavelengths λ is much larger than the plasma Debye length. Measurements in rarefied plasmas necessitate long

radar wavelengths. Jicamarca has measured incoherent scatter to altitudes of about 10,000 km and is also uniquely sensitive in the mesosphere where the electron number density is also small [*Farley*, 1991].

Another property of the incoherent scatter spectrum is the drastic narrowing that occurs for incidence nearly perpendicular to the geomagnetic field. In this case, the spectrum becomes much narrower than the ion thermal bandwidth, facilitating very accurate measurements of line-of-sight drifts. The phenomenon only occurs when $\lambda > 4\pi\rho_e$, where ρ_e is the electron gyroradius, and can only be observed when the radar beamwidth is very narrow and the backscatter signal is dominated by the part coming from small magnetic aspect angles [*Milla and Kudeki*, 2011].

Finally, high-power VHF radars can be used to study backscatter from fluctuations in the refractive index of neutral gases in the middle and lower atmosphere. MST radars are as important for studies of energetics, dynamics, and transport in the neutral atmosphere as incoherent scatter radars are in the ionosphere. With current technology and existing equipment, there need be no observing gap in altitudes between the boundary layer and the plasmapause.

The existing ISRs employ vacuum tubes, traveling-wave tubes, klystrons, or transistors for RF power. The power source is lumped in the first three cases and distributed in the last case where transistors are typically situated very close to individual antenna elements. The conventional paradigm involves using pulsed transmitters with high peak-power levels and duty cycles ranging from a few percent to a few tens of percent. The duty cycle can be exploited to the greatest extent by using pulse compression schemes or pulse coding which

allows long pulses to behave, in some respects, like shorter but more powerful pulses. Pulse coding can also be used to make the radar instrument function or ambiguity function closer to ideal, facilitating spectral measurements that are at once well resolved in range and frequency. **Both random and determinstic pulse codes are in use at different ISRs on the basis, in part, of the availability of signal generation equipment.** The price paid for pulse compression is a reduction in sensitivity due to increased radar clutter.

Today's ISRs utilize both phased-array and mechanically-steered dish antennas. **Whereas the former allow for rapid steering, the latter can present attractive cost- and performance-tradeoffs with respect to sidelobes and the ability to steer to low elevation angles.** Phased arrays also offer flexibility with regard to the use of spaced-antenna methods, including interferometry and radar imaging. Subdividing the receive array for interferometry and imaging comes at the cost of sensitivity and has been used in a limited way with the two EISCAT ESR radars for studying the naturally-enhanced ion acoustic lines (NIELS). Interferometry and imaging are used routinely for studying coherent scatter with the modular phased array at Jicamarca.

The only multistatic ISR presently is the EISCAT mainland radar network which is tristatic. Multistatic radars offer the ability to measure vector drifts unambiguously. Since the EISCAT radars are mechanically steered, however, each scattering volume along the transmit radar beam must be interrogated by the receive antennas one altitude at a time. This seriously limits the cadence of experiments and the utility of the multistatic capability.

3. Overview of radio arrays

A new paradigm for radio exploration of geospace comes from the **radio astronomy** community where a new generation of radio arrays is being developed and deployed. The radio arrays exploit spatial diversity to the fullest extent, going beyond traditional beam-forming methods and utilizing all of the spatio-temporal information in radio signals from subjects under study by using large-scale sparse interferometer systems. The geospace radar concept involves combining radio arrays with discrete or distributed transmitters to study volume scatter from the upper atmosphere and beyond. The goal is the production of datasets which reveal the space-time structure of geospace phenomena unambiguously and in a way that can readily be compared with or assimilated into numerical models, including forecast models, as well as machine-learning algorithms.

Radio arrays have a long history in the arena of solar research. Reviewing some of the milestones in this area provides context for the geospace-radar concept. The Culgoora array consisted of ninety-six 13m-diameter mechanically steerable dishes, arranged in a circle 3 km in diameter. It operated in dual polarization at 80 and 160 MHz. It was designed for solar work and so did not attempt to suppress grating lobes so long as they were out of the solar field of view. It was responsible for much of our understanding of meter-wavelength radio bursts. The resolution was sufficient to measure scatter broadening of Type III radio bursts by coronal turbulence.

In the case of the CLRO, the array was configured as a 3 km "T" of log-spiral antennas, predominantly in a single circular polarization. It was designed for both solar and cosmic work, so grating lobe suppression was important. It was one of the first to use a digital

correlation receiver. Its resolution was comparable to Culgoora, but it covered a broader band with the log-spiral elements.

In the last couple of decades, astronomical radio arrays have evolved significantly. The resolving capabilities of most modern radio telescopes are realized in two different ways: beamforming and interferometry. Perhaps the simplest way for a telescope to beamform is through the use of a dish (typically parabolic or spherical). Dishes are expensive, both to build and to maintain, and costs increase dramatically with the size of the dish. However, beamforming can also be accomplished using an array of dipoles, where the signal from each element is delayed and the total is coherently summed, effectively synthesizing an aperture. Historically, the delay portion of phased-array beamforming was accomplished with physical delay lines and phase-shifters which are awkward to calibrate and maintain.

Unlike beamforming, interferometry by nature requires multiple elements. Voltage samples from each element in an interferometer are cross correlated with the voltages from other elements. The physical distance and orientation of each antenna pair makes them sensitive to different spatial frequencies in different orientations. These spatial-frequency measurements can be Fourier transformed and summed to form an image. This process is called synthesis imaging as the elements in the array are synthesizing points on an aperture. For an interferometer comprised of N elements, there are $N \times (N-1)/2$ unique cross-correlation products. Although phase shifting can be performed after the cross-correlation, delay compensation is necessary in broadband systems, and this remains awkward and expensive. In the past, the fact that the computational load increased like the number of elements squared prohibited many-element interferometers.

Recently, advancements in computational power have opened the door to both digital beamforming and large-N synthesis imaging. In particular, large arrays comprised of hundreds of dipoles can digitally steer multiple beams simultaneously across large bandwidths using off-the-shelf CPUs **and, in practice, GPUs. The adoption of GPUs** by the radio astronomy community has allowed for real-time, wide-band synthetic imaging with fields of view limited only by the beam pattern of an individual antenna elements. Delays are still necessary, but they simply imply a digital buffer. Furthermore, digital buffers can be large enough to store the entire RF signal for the duration of an event so that, when an event is detected, the entire buffer can be saved and reprocessed as necessary. Such an event might be a fast radio burst (FRB) in radio astronomy, but many such situations can also be imagined in geospace research. These advancements are revolutionizing radio astronomy, but the geospace and space-weather communities for the most part continue to use decades-old facilities that rely on single dish or delay-line technology.

LOFAR: The Low Frequency ARray (LOFAR), the largest radio telescope in the lower VHF band, was built and is operated by the Netherlands Institute for Radio Astronomy, ASTRON. LOFAR is comprised of individual stations, most of which are located in the Netherlands. Currently, there are 24 core stations located in Exloo, NL, 14 remote stations located across the Netherlands, and 12 international stations located across Europe. Each station includes both low band (10-80 MHz) and high band (120-240 MHz) arrays.

The low band antennas consist of two linear, orthogonal dipoles, each made of two copper wires. The dipoles are resonant at 60 MHz and drop in sensitivity away from this frequency. The low band arrays of the core and remote station include 48 low band an-

tennas, and the international stations include 96. Beamforming with an individual station is done electronically, allowing for fast beam steering with no moving parts. The beamformed time series are then sent to a correlator for high-resolution imaging [*van Haarlem et al.*, 2013].

KAIRA: The Kilpisjärvi Atmospheric Imaging Receiver Array (KAIRA) is a LOFAR station which was constructed in 2011 in Northern Finland. KAIRA has demonstrated successfully that modern, low-frequency, digital phased array radio telescopes can be highly versatile instruments for studying various geophysical phenomena in Earth's near space using radio remote sensing [*Vierinen et al.*, 2013; *McKay-Bukowski et al.*, 2015]. The frequency range of $\approx 10 - 240$ MHz is ideal for studies of the Earth's near space. At these frequencies, the radar cross-sections of mesospheric echoes, meteor trail, and head echoes are maximized. As stated above, lower frequencies also allow observing lower plasma densities due to Debye-length effects. At lower frequencies, radio propagation effects such as scintillation and absorption are also stronger, facilitating studies of these phenomena.

Due to the versatile nature of the underlying digital phased array technology, the same system can be used for a number of different active and passive geophysical radio remote sensing applications including phased array incoherent scatter radar [*Vierinen et al.*, 2013; *Virtanen et al.*, 2014], spectral riometry [*Kero et al.*, 2014], multi-static studies of the mesosphere [*Chau et al.*, 2018a], and for characterization of wide-band ionospheric scintillation [*Fallows et al.*, 2014].

One of the strengths of the all-digital phased array technology is the wide bandwidth. This allows multi-wavelength studies of various plasma physics phenomena in geospace.

The refractive index for ionospheric plasma is frequency dependent. The same applies for radar cross-sections of various phenomena such as meteor head echoes and mesospheric echoes. So far, the information from simultaneous, multi-wavelength observations has remained relatively unexplored. Due to the wide band nature, KAIRA can actually be used together with multiple radar transmitters as a phased array radar receiver. So far, it has been used together with the EISCAT VHF transmitter, the MAARSY MST radar, and the Andøya meteor radar. Therefore, another strength of using modern radio arrays is that they can be used together with a range of existing and planned radar transmitters as a multi-static platform.

MWA: The MWA consists of 2048 dual-polarization dipole antennas optimized for the 80-300 MHz frequency range, arranged as 128 "tiles", each a 4×4 array of dipoles. The array has no moving parts, and all telescope functions including pointing are performed by electronic manipulation of dipole signals, each of which contains information from nearly four steradians of sky centered on the zenith. Each tile performs an analog beamforming operation, narrowing the field of view to a fully steerable 25 degrees at 150 MHz.

The majority of the tiles (112) are scattered across a roughly 1.5 km core region, forming an array with very high imaging quality, and a field of view of several hundred square degrees at a resolution of several arcminutes. The remaining 16 tiles are placed at locations outside the core, yielding baseline distances of about 3 km to allow higher angular resolution for solar burst measurements.

Important ionospheric research has already been peformed with the MWA. In particular, *Loi et al.* [2015] recently identified field-aligned ionization ducts between the ionosphere and the plasmasphere in spatially-resolved maps of total electron content (TEC).

LWA: The Long Wavelength Array (LWA) is a concept for an HF/VHF radio telescope comprised of 52 stations spread over the state of New Mexico, providing 0.4 km^2 of collecting area. With baselines ranging from a few km up to about 400 km, such a radio telescope could achieve down to 5 arc second resolution.

A single LWA station is comprised of 256 dual polarization, bow tie antennas pseudo-randomly spread over a 100x110 m ellipse. The antennas are slightly bent to achieve greater sensitivity to a wider range of zenith angles. A single station can act as a 256-element interferometer, capable of imaging nearly the entire visible sky, or as a digital beamformer, capable of producing several beams at once.

To date, two stations have been completed in New Mexico. The first station, LWA1, is collocated with the Very Large Array and operates from 10-88 MHz [*Ellingson et al.*, 2012]. The second station, LWA-SV, which is located at Sevilleta National Wildlife refuge, is operationally nearly identical to LWA1 except it has modified analog filters allowing observations down to 3 MHz.

Furthermore, the digital processor on LWA-SV has been upgraded from LWA1 to make use of graphics processing units (GPUs) through the Python/C++ Framework known as Bifrost [*Cranmer et al.*, 2017]. GPUs are capable of performing large numbers of basic calculations simultaneously, making them ideal for radio arrays comprised of many, non-uniformly distributed elements such as an LWA station. Bifrost is designed to work

on streaming data such as radio array voltages in real time and allows for rapid pipeline development with its high-level python interface.

LWA at Owens Valley Observatory (LWA-OVRO) is a higher resolution LWA telescope built for monitoring of astrophysical transients. With maximum baselines of 100 m, LWA1 and LWA-SV achieve a synthesized beam full width at half the maximum (FWHM) of a few degrees in the lower VHF band. However with maximum baselines of 1.5 km, LWA-OVRO is capable of imaging the entire sky at a resolution of a few 10s of arcmin.

EISCAT_3D: EISCAT 3D is a next generation all-digital multi-static phased array radar which is currently being constructed in Northern Scandinavia [*McCrea et al.*, 2015]. The core transmit-receive site will be located in Skibotn. Two outlier receive-only system are to be located in Sweden and Finland, approximately 150-km distance from Skibotn. Each one of the sites consists of 109 modules, with 91 antennas in each module. The operating frequency is 233 MHz. The transmit power will be 5 MW peak power with a 25% duty-cycle.

The main novelty of EISCAT 3D is that it will have the capability of observing vector ion velocities simultaneously at all altitudes by using multiple bistatic beams that intersect the transmit beam. Due to the rapid beam switching capability, the radar will be able to perform a volumetric observation quickly. EISCAT 3D will also enable aperture-synthesis radar imaging in order to improve spatial resolution of auroral radar observations, a technique that has been used already for a long time at the Jicamarca Radio Observatory (e.g. *Hysell and Chau* [2006]).

Once finished, EISCAT 3D will be the most modern incoherent scatter radar in the world. By virtue of its frequency and its latitude, it will not, however, be able to fulfill all of the objectives of a geospace radar as laid out in this paper. Unlike LWA or LOFAR, the EISCAT 3D receiver array is also relatively narrow band (30 MHz), limiting the applicability of the radio array for uses other than 233-MHz radar operations.

4. Capabilities of modern radio arrays paired with HPLA transmitters

In this section, we summarize some of the existing and potential capabilities that modern radio arrays would bring to geospace research operating in radar mode, particularly in the low-VHF band. To keep our summary focused, we assume a large radio array for transmission and multiple, spatially separated radio arrays for reception. In this respect, we start with the transmitting capabilities and continue with the receiving capabilities and the motivation for focusing on the low-VHF band.

4.1. Transmitter capabilities

Recent developments in technology allow the possibility of large transmitting arrays with solid-state transmitters possibly at each antenna element. Solid-state technology in conjunction with contemporary, compact antenna element designs (e.g., LWA), would allow operations over a relatively broad band at low VHF frequencies. Moreover, modern designs would allow larger duty cycles and even continuous wave (CW) operation. This implies an increase in average power even for systems that are peak-power limited. The result is the ability to probe a broader range of geospace.

Although performance advantages of a distributed transmitter are clear, radar users are well-aware that much of the costs of operating a radar are in operating and maintaining the transmitter. It is this that limits the operating hours of many ISRs. By comparison, a distributed transmitter **might be expected to pose fewer maintenance challenges over time** and permit 24/7 operation at little additional cost.

The possibility of a transmitter on each antenna, and depending on the RCS of the desired target, allows:

- Fast beam steering to reduce space-time ambiguity.
- Multiple, simultaneous beam pointing directions for multi-target, multi-use applications [*Milla et al.*, 2013].
- Antenna compression to generate beams with different widths [*Woodman and Chau*, 2001; *Chau et al.*, 2009].
- Implementation of multi-frequency approaches to improve range resolution (range imaging).
- Implementation of coherent MIMO configurations using code diversity [*Urco et al.*, 2018a]. Coherent MIMO can be used to take advantage of the spatial information arising from distributed transmitter modules .
- Implementation of low-power modes, either for long-term operations or for strong targets.

In the last 10 years, great progress has been made with **broadband** phased array radio telescopes. There would be great benefit from a matching frequency-agile transmit capability. This would allow radar studies of space plasma physics phenomena with one additional

independent variable: frequency. This information would be useful, e.g., for studies of atmospheric turbulence spectra and determining the sizes of meteor head echoes. For solar radar, this would allow studies of the solar corona at different depths [*Bastian*, 2003, 2004].

4.2. Receiver capabilities

In the case of receivers, based on the recent developments in radio astronomy (e.g., LOFAR, LWA), monostatic and multistatic configurations would provide significant new capabilities to a geospace radar. Much like a radio telescope, a geospace radar receiver could leverage the power and flexibility of software controlled beamforming and aperture synthesis imaging. Furthermore, a radio astronomy-like digital processor could easily be modified for flexible radar processing and data acquisition. This has already been demonstrated with LOFAR [*Vierinen et al.*, 2013] and LWA [*Taylor*, 2014].

The new capabilities for reception, related to the transmitter capabilities described above but not limited to them, would include:

- Many simultaneous independent beam pointing directions available at all times. This allows, e.g., different altitudes to be sampled simultaneously by a multistatic receiver and many other presently impossible operational modes.
- Multistatic reception capability for resolving three-dimensional flows unambiguously.
- Antenna compression to generate beams with different widths on reception.
- Implementation of synthetic aperture imaging by utilizing smaller sections within receiving arrays or combining spatially separated receiving arrays (e.g., LOFAR core).

373 • Implementation of coherent MISO, i.e., single antennas (or group of antennas) could
374 be used for interferometric/imaging purposes if the target is sufficiently strong.

375 • Broadband interference identification and rejection from sources such as lightning
376 and solar radio bursts.

377 The theme of these capabilities is the exploitation of spatial diversity to resolve features
378 and flows in three dimensions, expanding the domain of geospace radar observations be-
379 yond simple profiling and conventional monostatic beam forming. The applications iden-
380 tified below exemplify the need for the capabilities specifically.

4.3. Why low-band VHF?

381 **There are clear disadvantages associated with operating in the VHF band. Lower**
382 **frequencies imply larger array sizes, greater material costs,and and greater demands**
383 **on real estate. Licensing in the VHF band may also be difficult in some contries. Most**
384 **importantly, increased galactic noise at VHF compared to UHF impies challenges for**
385 **system sensitivity and a potential requirement for greater transmitter power. The sen-**
386 **sitivity problem is mitigated partly by reduced atmospheric absorption and cabling**
387 **losses.**

388 Despite these problems, most of the geospace-radar applications above would benefit
389 from using low-band VHF. In terms of feasibility, the technology needed for a low-band
390 VHF geospace radar is already proven; the required antennas, digital receivers, beam for-
391 mers (based on FPGA), and solid-state transmitters are available commercially now. A
392 number of other factors make low-band VHF advantageous. For example, radio frequency
393 interference (RFI) in the low band VHF can be a limiting factor for receiving arrays. How-

ever, as shown by both LOFAR [*van Haarlem et al.*, 2013] and LWA1 [*Ellingson et al.*, 2012], the spectrum between 30 and 80 MHz is relatively clean, even in densely populated countries like the Netherlands. Other noteworthy factors related to low-band VHF radar are summarized in the following list:

- Radio propagation effects of interest such as Faraday rotation and scintillation are stronger at low VHF frequencies.
- Array element patterns are broader in the low VHF band. This allows any fully-digital low-band receiving array to have an unlimited number of beams covering the entire visible hemisphere at no penalty in signal-to-noise ratio.
- The radar cross-sections of many of the phenomena of interest are also larger.
- Finite Debye-length effects for ISR impose less severe limitations on the minimum detectable electron number density.
- Planetary (Lunar) studies would benefit from deeper subsurface penetration at VHF.
- The power spectral density of galactic synchrotron emission as a function of frequency is proportional to $f^{-2.5}$ [*Rogers and Bowman*, 2008]. However, the bandwidth of the incoherent scatter ion line, and therefore the minimum receiver noise bandwidth, is proportional to f. This means that the signal to noise ratio for the ion-line is not as strongly dependent on frequency as one would expect by just looking at the sky noise: $\mathrm{SNR}(f) \propto f^{1.5}$.

5. Geospace radar applications

In this section, we describe some of the possible applications of a new geospace radar, starting from the lower atmosphere and ending at the Sun. The applications are meant to be illustrative rather than exhaustive. New applications will emerge as novel remote sensing approaches designed for the current applications mature.

5.1. MST applications

The neutral atmosphere can be also studied with VHF radars in so-called MST mode. The first application of such radars for neutral atmospheric dynamics was conducted at Jicamarca [*Woodman and Guillén*, 1974]. Since then, the MST technique proliferated world-wide, with small systems covering the altitudes between a few hundred meters to lower stratospheric altitudes (i.e., less than 20 km). The altitudinal coverage of these systems depends on the frequency of operation, size of the antennas, and transmitting power. The corresponding systems are called boundary layer radars, wind profilers, and ST radars [*Hocking*, 2011]. In the case of the mesosphere, there is a handful of HPLA radars working between 45 and 55 MHz, able to receive echoes from irregularities embedded in neutral turbulent layers (e.g., Jicamarca, Gadanki, MU, MAARSY). At high latitudes, due to the presence of charged ice particles during the summer, smaller systems are being used to study the polar summer mesosphere from so-called polar mesospheric summer echoes (PMSE). In all these cases, low VHF frequencies have been used to study the neutral atmosphere from a few hundred meters to the lower stratosphere and in some parts of the mesosphere depending on the latitude, time of the day, and season.

The region between the lower stratosphere and the lower mesosphere (i.e., between 20 and 55 km) has been known as the "radar gap region" since this region typically cannot be observed with existing radars. Using long integration times and dual polarizations at Jicamarca, *Maekawa et al.* [1993] reported on atmospheric echoes from this region for the first time.

A modern and powerful geospace radar should be able to sample the whole MST region by combining low-power modes for the lower atmosphere with high-power modes for the stratosphere and mesosphere. The stratosphere and lower mesosphere is the region where primary gravity waves are expected to break and dissipate, modify the background conditions, and generate so-called secondary gravity waves.

The daytime exploration of the mesosphere could be also complemented with ISR observations of the D region. Although radar scattering is from electrons, the collision frequency at these altitudes is so high that the dynamics of the measured spectra are dominated by the neutrals. Using the Poker Flat Incoherent Scatter Radar (PFISR) during a strong auroral precipitation event, *Nicolls et al.* [2010] were able to study inertial gravity waves that had originated a few days before at the surface a few thousand kilometers away. In the case of a powerful geospace radar, such atmospheric events could be studied during the daytime routinely, i.e., without the need of strong electron density enhancements.

Besides exploring a new altitudinal region, a modern geospace radar could be used to explore the MST region with larger horizontal coverage and greater altitudinal, horizontal, and temporal resolution than is presently possible. Such improvements would allow the combination of radar imaging, range imaging, multi-static observations, and MIMO

implementations. Recently, *Urco et al.* [2018b] observed PMSE with unprecedented horizontal resolution using a combination of Maximum Entropy and MIMO techniques. The resolution achieved with the MAARSY 90-m diameter antenna was equivalent as to having a 450-m diameter array. The resulting images show that the summer polar mesosphere presents rich spatial and temporal structures associated to a combination of vertically propagating waves from below, horizontally drifting waves, and instabilities and waves generated in situ. Figure 1 shows an example of such 3D images obtained with 40 second integrations: (a) a horizontal cut at 85.80 km, (b) an altitude vs zonal direction cut, and (c) an altitude vs meridional cut, color-coded with Doppler velocity, spectral width and intensity information. A powerful geospace radar would allow similar mesospheric observations at low and middle latitudes where mesospheric echoes are mainly dependent on atmospheric turbulence and therefore have an RCS a couple of orders of magnitude smaller than PMSE.

The horizontal coverage can be extended, in the case of lower atmospheric altitudes where the echoes are stronger, by using smaller sections of the transmitter array, different pointing directions, and multi-static configurations.

5.2. Meteor science and applications

In the mesosphere and lower thermosphere (MLT), i.e., between 70 and 120 km, echoes from meteors can be also observed with low VHF-band radars. There are three main types of meteor echoes: (a) specular trail echoes due to Fresnel scattering when the radar points perpendicular to the meteor trajectory, (b) Head echoes coming from plasma as it forms in front of the meteoroid, and (c) non-specular trail echoes, also known as range-spread

trail echoes resulting from the combination of field-aligned irregularities and charged dust particles.

Meteor echoes have been used to study meteoroid composition, origin, and masses, and to explore the MLT region. Traditional specular meteor echoes have been used since the 1950s to explore the MLT dynamics with small radars systems called specular meteor radars (SMRs). They are typically composed of one wide-beam transmitting antenna and a receiver interferometer operating between 30 and 50 MHz. Recently, such systems have been improved using multi-static geometries, coded CW transmissions, and MIMO configurations [*Stober and Chau*, 2015; *Vierinen et al.*, 2016; *Chau et al.*, 2018b]. The improvements allow such systems to measure the MLT wind fields with much larger horizontal coverage and resolution as well as improved vertical and temporal resolutions [*Stober et al.*, 2018]. Current efforts are being devoted to determining the second order statistics of the wind field as function of wavenumber (horizontal and vertical) as well as frequency.

A powerful geospace radar would allow the detection of much weaker signals due to meteoroids with less mass or smaller entry speeds. One of the outstanding questions in aeronomy is how much meteor mass is deposited in the atmosphere? So far, different methods provide estimates with a couple of orders of magnitude spread. A geospace radar could greatly improve the measurements of the lower mass/speed end of the spectrum, from both head as well as specular meteor echoes.

In the case of head echoes, only HPLA radars with interferometry are able to determine precisely the meteoroid trajectory and where in the beam such echoes occur, something crucial for the scattering meteor mass determination. So far, such measurements have been

conducted only at Jicamarca, MU, and MAARSY using narrow beam configurations [*Chau et al.*, 2007; *Kero et al.*, 2011; *Schult et al.*, 2017]. The use of a wider beam, longer duty cycle sequences, and MIMO configurations would improve significantly the detection and characterization of such echoes.

Non-specular meteor echoes are still enigmatic since they appear to result from a combination of field-aligned irregularities and charged dust particles. A clear indication of the former comes from observations at low and mid latitudes where these relatively long-lived range-spread echoes come primarily when the beam points perpendicular to B. The latter come from high latitude observations where perpendicular-to-B observations are not possible. Besides the interest in understanding the physics behind these echoes, they can be used to get precise altitudinal profiles of MLT winds with high temporal and spatial resolution [*Oppenheim et al.*, 2009]. The proposed geospace radar, if located at low or mid latitudes, would be able to provide such measurements on routine basis, contributing further to the complicated atmospheric dynamics of the MLT region. Besides routine observations of these profiles, the horizontal coverage would be improved by using multi-static and multi-beam approaches.

5.3. Ionospheric research

Since its inception, the incoherent scatter technique has provided the most incisive measurements of ionospheric state parameters available through ground-based remote sensing. These include plasma number densities, temperatures, composition, and line-of-sight drifts as well as information about the electron energy distribution and inferences about the state of the neutral atmosphere. Most of the information has come in the form of profiles ob-

517 tained along the beam pointing direction of the radar. Profiles are useful in view of the fact
518 that the ionosphere is vertically stratified. Volumetric information came mainly from me-
519 chanical beam steering before the emergence of the Advanced Modular Incoherent Scatter
520 Radars (AMISRs) currently deployed in Alaska and Canada which employ electrically-
521 steered phased arrays.

522 The importance of obtaining volumetric information is highlighted by Figs. 2 and 3
523 which represent radar observations of plasma density irregularities associated with plasma
524 convective instability at low magnetic latitudes and so-called "equatorial spread *F*." Fig. 2
525 was obtained by the ALTAIR radar in the Marshall Islands and shows an east-west scan
526 acquired at pointing angles a few degrees away from perpendicular to the geomagnetic
527 field. The figure exhibits large-scale undulations in the *F*-region bottomside along with
528 depletion plumes penetrating through the *F* peak and into the topside. The irregularities
529 evolve on timescales of a few minutes or tens of minutes which is comparable to the time
530 required to complete a scan. Although informative, the figure is not a true image and is
531 highly distorted.

532 Fig 3 shows data acquired a few minutes earlier along antenna pointing positions pre-
533 cisely perpendicular to the geomagnetic field. Patches of intense backscatter concentrated
534 in the depleted regions in Fig. 2 represent coherent scatter or Bragg scatter from small-
535 scale field-aligned plasma density irregularities. Like the large-scale irregularities evident
536 in Fig. 2, the small-scale irregularities are a consequence of plasma instability and signify
537 the presence of free energy in the ionosphere. They are a vivid manifestation of space

weather and a hazard for radio communication, navigation, and imaging systems operating at low geomagnetic latitudes.

The coherent scatter conveys information about the the underlying plasma instabilities that is highly complementary with the incoherent scatter which conveys information about plasma state variables. Ideally, we would like to acquire signals from the entire ionospheric volume within the figure simultaneously, including from both large and small magnetic aspect angles. This would be true imaging and would permit direct, unambiguous comparison with direct numerical simulations.

One of the major shortcomings of the ALTAIR data in Figs. 2 and 3 is the absence of reliable drifts measurements. Plasma drifts at the geomagnetic equator are relatively small, and the incoherent integration time necessary to acquire and formulate accurate drifts measurements in this case is longer than the timescale along which the large-scale plasma irregularities evolve. The measurement is not stationary at UHF frequencies. At low VHF frequencies, and for beam pointing angles very close to perpendicular to the magnetic field, accuracy of ISR drifts measurements improves dramatically, and the measurements become stationary. This is a strong argument for favoring low VHF frequencies for a geospace radar.

The high quality of ISR drifts obtained with beams pointing perpendicular to the magnetic field is due to the narrowness of the ISR spectrum at low VHF frequencies allowing the application of Doppler-shift detection to estimate the drifts. The narrowness of the spectrum is caused by the relatively long temporal correlation of the field-aligned electron density fluctuations that diffuse slowly across the magnetic field lines. Such diffusion is

not dominated by Landau damping but by Coulomb collisions. Incoherent scatter theory has been reformulated recently to incorporate the effects of Coulomb collisions on particle dynamics by describing the statistics of electron and ion trajectories using a Fokker-Planck kinetic equation with speed-dependent friction and diffusion coefficients. Measurements with the Jicamarca radar at 50 MHz have been shown to agree with the proposed theory. However, the validation is limited since only a single radar frequency has been used in a particular configuration. A modern geospace radar would let us to conduct similar tests to study the effects of Coulomb collisions on ISR signals at multiple radar frequencies, magnetic aspect angles, and antenna beam widths for different ionospheric altitudes including topside regions where plasma composition would impose another level of complexity. This study is of general relevance as a test for theoretical plasma physics.

5.4. Plasmaspheric research

A problem was discovered recently with the standard high-altitude ISR mode at Jicamarca. Samples acquired from very high altitudes were being used as the basis for noise estimates. From time to time, however, the noise estimates became contaminated. Upon closer examination, the contamination was found to be due to coherent scatter from high altitudes just above 2000 km. This is the altitude where the on-axis antenna pointing position at Jicamarca was perpendicular to B at the time. High-altitude field-aligned irregularities were the cause. The irregularities occurred mainly in the pre-dawn sector. The immediate problem was solved by using samples taken during transmitter-off intervals for noise estimates. The problem of the origin of the high-altitude field-aligned irregularities remains.

An example of the phenomenon in question is shown in Fig. 4. The figure was generated by computing the modulus of the longest lag in the measured ISR lag-product profiles, 1.5 ms, which should be essentially zero for incoherent scatter. The experiment in question is very sensitive compared to more conventional coherent scatter experiments, and the echoes were not very strong compared to what is received from the electrojet or equatorial spread *F*. The coherent scatter occurred in layers that migrated in altitude slowly in time. Since the experimental geometry favored field-aligned echoes between about 2000-2500 km in this case, we do not know the true altitude span of the irregularities.

Subsequent discussions revealed that this phenomenon had been known since the earliest days of Jicamarca (personal communication, D. T. Farley, J. P. McClure). However, it was not deemed to be as interesting as the other ionospheric phenomena being discovered in the 1960s and was never pursued. Contemporary ISR experiments designed to remove outliers arising from different kinds of radar clutter masked the phenomenon which was only rediscovered by accident.

The high-altitude coherent scatter is significant since it signifies the presence of an unknown source of free energy and an unknown plasma instability. The echoes are not merely high-altitude examples of FAIs caused by equatorial spread *F* which can occur above 2000 km altitude during periods of high solar flux under geomagnetically-disturbed conditions. The echoes in Fig. 4 occurred during a period of low solar flux and quiet conditions. They were not preceded by spread *F* and occurred during June solstice when spread *F* is relatively uncommon. That they occur mainly in the pre-dawn sector suggests that beam

instabilities driven by photoelectrons may be playing a role. To test the hypothesis, dedicated rather than serendipitous observations are required.

5.5. Planetary research

Low frequencies are especially useful for probing the subsurface of dielectric bodies. The penetration depth of an electromagnetic field is inversely proportional to frequency. Lower frequencies are used in Earth remote sensing for applications such as hydrology and foliage-penetrating radar. In the case of planetary exploration, low frequency observations are used to probe the subsurface of planetary bodies, e.g., in search of subsurface ice deposits on Mars or ice on permanently shadowed craters on the Moon. In general, radar observations across a number of different frequencies can yield a great deal of information on the geological surface and subsurface composition and structure of planetary bodies.

With a geospace radar, the only planetary body that can be mapped with good resolution is the Moon. The Moon is close enough that high signal-to-noise ratios can be achieved. It is also large enough that the target size in range and Doppler shift permits a large number of measurement points. Contemporary 6-meter wavelength radar mapping efforts achieved approximately a 15x15 km resolution which is limited by ionospheric scintillations and the limited tracking time possible. With a more flexible low frequency radar, it is plausible to obtain range-Doppler resolution of approximately **1.5 km** $\times$ **1.5 km** per pixel with good ionospheric conditions from a non equatorial location.

A low frequency polarimetric inverse synthetic aperture radar image of the Moon obtained at Jicamarca [*Vierinen et al.*, 2017] is shown in figure 5. This 49.92 MHz radar image is the lowest frequency polarimetric synthetic aperture map of the Moon that has

been made, allowing us to peer deeper beneath the surface of the Moon than before. This frequency is close to the lowest possible frequency that can be used for a ground based observation due to deleterious effects of ionospheric scintillation and other radio propagation effects.

The 6-meter wavelength radar map provides a unique view of the Moon. Resonant scattering from Breccia in the vicinity of newer impact craters allows us to infer the amount of large blocky material. These regions appear radar bright. Examples of such regions include the area in and around the Copernicus and Tycho craters. The bulk radar brightness on the other hand allows us to infer the dielectric properties of the subsurface. Lossy FeO and TiO2 rich mare regions of the Moon have a larger loss tangent and appear radar dark while low loss terrae regions appear radar bright.

One of the key findings of the 6-meter wavelength study [*Vierinen et al.*, 2017] was the discovery of a large radar dark region which joins Mare Frigoris and Mare Imbrium. This finding supports the hypothesis that Mare Imbrium and Mare Frigoris are part of the same impact basin – one of the largest impact basins on the Moon. The other key finding was the radar dark Schiller-Zucchius impact basin on the southern hemisphere of the Moon. This can be seen on the top-right panel of Figure 5. The radar observation supports the hypothesis that this old impact basin is associated with basaltic flows which are now mostly covered by optically bright terrae material produced by newer impact ejecta. These recent findings show that low frequency planetary radar, which peers beneath the visible surface of the Moon, can provide important new information about the geological formation of the Moon which is still poorly understood.

5.6. Solar research

The cause celebre for geospace radar could well be solar research. The ability to receive soundings from the sun with ground-based radar would represent a new avenue for studying solar physics. It could expedite the creation of an operational space-weather forecast strategy involving tracking along with prediction of CME trajectories. Finally, it would unify the solar, magnetospheric, and ionospheric research communities under a common observational paradigm. The concept is not new and is not simple but appears to be plausible using available dual-use technology.

5.6.1. Historical background

Since the start of the planetary-radar era, multiple attempts have been made to detect radar reflections (soundings) from the solar corona. The first, in 1959, was by a Stanford University group working at 25.6 MHz [*Eshleman et al.*, 1960]. Eshleman reported detecting echoes at 1.7 solar radii after 36 min. of integration using a monostatic radar system with 25 dB of antenna gain and 40 kW average power. The results were deemed to be consistent with expectations for an ideal, conducting sphere at the time but could not be repeated.

Subsequently, a major, multi-year effort was undertaken by a group from MIT using a dedicated 38.25 MHz radar built in El Campo, Texas [*James*, 1964, 1970] and operated continuously from 1960 to 1969. The average power and gain of the El Campo radar were 500 kW and 33–36 dB, respectively. These are very impressive specifications for what would be a temporary, short-lived radar facility. Highly variable echoes (in terms of power, Doppler shift, and bandwidth) were reported. Several analysts attributed the

variable echoes not to critical-frequency reflection but to coherent scatter from one or more electrostatic plasma waves (e.g. [*Khotyaintsev*, 2005]). Despite the unexpected variability of the signals, at the time and for decades thereafter, the El Campo results were considered to be reliable and definitive if not particularly well documented proof of the solar-radar concept. **The results have not been replicated, in part due the the absence of a suitable facility for performing the experiments.**

Another attempt was made at Arecibo in 1966 and 1967, using a 40-MHz, 50/100 kW average power transmitter [*Parrish*, 1968]. The gain of the Arecibo system at 40 MHz was 37 dB. The investigators duplicated the experimental mode utilized earlier at Stanford. While preliminary work suggested that solar echoes were detectable, and while positive results were again obtained when the experiments were repeated, the results were never published. The perceived lack of novelty rather than any shortcomings in the research kept the results from the literature (D. Campbell, 2016, personal communication.) The 40-MHz transmitter was decommissioned, and no further attempts have been made at Arecibo.

In 1996, solar radar experiments were attempted in the FSU using the SURA heater in Russia as a transmitter and the UTR-2 radio telescope in Ukraine as a receiver [*Rodrigues*, 2013]. The study was not comprehensive, and the findings were neither conclusive nor well documented.

Most recently, solar radar experiments were attempted repeatedly at Jicamarca during a multi-year study [*Coles et al.*, 2006]. An unsuccessful attempt to observe solar echoes at Jicamarca was actually made back in 1964, but it was not documented (personal communication, K. Bowles, B. Balsley, and D. Farley). In the recent experiments, the average power

688 and antenna gain were about 112 kW and 41.6 dB, respectively. After a thorough statistical
689 analysis of the data, no clear, unambiguous echoes were found, and the upper bound on the
690 solar cross section was reduced to a figure below that implied El Campo observations. The
691 implication of the study was that the echoes reported from El Campo might have been spu-
692 rious and associated with solar radio bursts rather than radar reflections. This conclusion
693 is controversial and does not explain the Arecibo results.

694 **5.6.2. Experimental demands**

695 As mentioned above, for solar, magnetospheric, and plasmaspheric studies, the radar
696 wavelength must be longer than the plasma Debye length. This places a premium on low
697 radar frequencies which overrides the penalty of increased sky noise. However, the radar
698 frequency should not fall below the maximum usable frequency (MUF) since that would
699 invite radar clutter from sky waves. The ideal frequency is therefore between 40–50 MHz.
700 Some additional frequency considerations are discussed below.

The simple figure of merit described below is not appropriate for optimizing solar radar experiments in which the transmit and receive antenna specifications need to be be considered separately. Optimum array sizes are determined by the power budget for solar echoes. The radar equation can be used to estimate the received signal flux:

$$S_r \;=\; P_t G_t L_p \sigma_r / (4\pi r^2)^2 \tag{2}$$

where P_t is the transmitted power, G_t is the gain of the transmitting antenna, L_p is the two-way loss factor for absorption in the lower corona, σ_r is the solar radar cross section,

and r is the solar distance. The noise flux is similarly given by

$$S_s = KT_s\Omega_s B/\lambda^2 \tag{3}$$

where K is Boltzmann's constant, T_s is the solar noise temperature, B is the bandwidth, and λ is the wavelength. The symbol Ω_s is the solid angle subtended by the Sun. It is assumed here that the Sun nearly (but not entirely) fills the field of view of the radar and that all of the noise sources outside the Sun may be neglected. Taking the ratio of Eqs. 2 and 3 gives the anticipated signal-to-noise ratio

$$\mathrm{SNR} \;=\; P_t A_t L_p \epsilon_s/(4\pi r^2 K T_s B) \tag{4}$$

in which A_t is the transmitting antenna effective area and ϵ_s is the scattering efficiency of the Sun **(the ratio of the scattering cross section to the physical cross section)**, which is assumed to be fully illuminated.

Estimating the factors in Eq. 4 is challenging since solar echo detection remains to be demonstrated and since a mode capable of detecting them remains to be defined. The effective bandwidth of the experiments at Jicamarca following coherent processing is 1 kHz. ***James*** **[1970] estimated the loss factor L_p to be about 3 dB, although that figure is probably an underestimate (see** ***Coles*** **[2004];** ***Coles et al.*** **[2006] and references therein). The noise temperature of the quiet sun at 50 MHz is of the order of 10^6 K, although the actual system noise is dominated by solar radio bursts as discussed below.**

The crucial performance metric is the transmitter power-aperture product which sets the flux that can be delivered to the Sun. In order to optimize this flux, the antenna for

transmission should be a steerable aperture or filled array at least comparable in size to Jicamarca's. Steerability is necessary to keep the radar beam trained on the Sun, facilitating long incoherent integration times.

Remarkably, the receive-array size does not enter into the calculation. In fact, the receive array must be large enough that most of the noise it receives comes from the solar disk itself and not from the galactic background. This assumption, which is not difficult to satisfy in practice, is built into eq. 4. Moreover, we have to consider that the main source of noise in solar radar experiments will be solar radio bursts.

Observations of the Sun at meter wavelengths with Culgoora and CLRO have shown that the various radio burst (Types I, II, III, IV, etc) have at least 20 dB and often 30 dB higher brightness than the quiet Sun. The most common burst, type III, comes from a small region and is broadened by scattering in the corona to angular size of order 3 arc min at 80 MHz. When the radar receiver beam covers the whole Sun, as it did in the early solar radar experiments, these bursts dominate the system noise temperature by a large factor. Accordingly, a solar radar receiver must be able to resolve type III bursts so that the receive beam can be directed to the quiet Sun between the bursts. In fact it would be preferable to design the receive beam to have nulls at the position of the type III bursts, implying the need for a maximum likelihood beam-former. However the antenna must be capable of resolving the burst in order to put a null on it and to perform imaging with very high dynamics range [*Oberoi et al.*, 2018; *Mondal et al.*, 2018; *Sharma et al.*, 2018].

These considerations suggest that a suitable receiving antenna will be a phased array with an aperture of order 10 km in diameter and a beam-former that can form multiple

simultaneous beams with very low sidelobes. However, special efforts to suppress grating lobes will not be necessary since the Sun is by far the most powerful noise source in the Sky, and very low-noise receivers will not be required. Instead, the receivers must be optimized for high dynamic range and good stability. Good calibration and good stability will be required to minimize sidelobes.

5.6.3. Solar-radar opportunity

The possibility of observing not only the sun but also solar arcs and coronal mass ejections (CMEs) with ground-based radar remains an attractive scientific objective and an important impetus for this project. A solar-radar capability could possibly be used to estimate the range, bearing, and speed of a CME. Such information could form the basis of practical space weather event forecasts. It could also supply critical information to more conventional model-based forecasts, including information about the coronal magnetic field inferred from Faraday rotation.

6. Facility capabilities and requirements

Table 1 summarizes the capabilities of a geospace radar which would be able to pursue the research objectives described above. The categories in the table are broad, and the delineations are somewhat artificial, as most of the radar's capabilities would be exploited in every avenue of research over time as the research matures. The table does show how progress across a broad span of geospace science would follow from the pursuit of the geospace-radar concept.

Most every scientific application requires high peak power of the order of one to several MW. Additional sensitivity would come from high average power or even CW operations involving the transmission of long pulse codes. Sensitivity will be critical for applications where either transmission or reception occurs on subarrays of the main antenna array, for example in MIMO and imaging applications. High average power is important especially for estimating meteoric mass flux and for probing distant targets, the solar corona most acutely. High duty cycles are a cost-effective strategy for achieving high average power and good sensitivity in view of the fact that costs are driven largely by peak power.

Multistatic observations are the only way to measure vector drifts unambiguously and are important for every avenue of geospace research except perhaps planetary radar. The contemporary practice of inferring three-dimensional flow fields from monostatic line-of-sight drift measurements is impeding our understanding of the complex dynamics found throughout the upper atmosphere. The ability to track CMEs with multistatic solar radar would provide an incisive tool for space-weather forecasting.

Distributed, modular receive arrays supported by multichannel receivers are central to the radio-array concept and the foundation of true radio and radar imaging. More than any other capability, the modern geospace radar would rely upon distributed spatial sensing to unravel space-time ambiguity and reveal the three-dimensional structure of targets and features in the upper atmosphere, the plasmasphere, and the solar corona. While planetary radars derive imaging information from the Doppler shift, interferometry is essential for disambiguating echoes from the northern and southern hemispheres.

776 Both multi-static and distributed modular arrays could be implemented with current tech-
777 nology used in modern radio arrays, e.g., LOFAR, LWA, MWA. To use such systems as
778 receivers of the proposed main transmitter array, the capability to record signals centered
779 around the frequencies of interest is needed. Such capability has been proven already at
780 KAIRA, LOFAR International, and LWA-SV, receiving signals from transmitters operat-
781 ing from a few MHz to 54 MHz. In the case of solar-radar applications, an array of arrays
782 with spacings up to 10 km or so, like LOFAR-core (e.g., *Kontar et al.* [2017]), would be
783 needed. To be able to get both high resolution images of solar radio burst and solar radar
784 echoes, the pre-combined complex signals of each array need to be recorded so that spatial
785 autocorrelation functions are available and, from them, the brightness of solar burst as well
786 as of solar echoes. Complex voltages would be needed to accommodate the transmitter
787 modulation.

788 Full polarization diversity is absent in all of the current ISRs with the exception of Jica-
789 marca. Polarimetry is used there now to measure Faraday rotation which serves as means of
790 calibrating ISR power measurements absolutely. Echoes from meteors and from the plan-
791 ets can also be polarized due to incidences of multiple scatter. The polarization of meteor
792 echoes in particular is an important source of information about the scattering mechanism
793 that has been largely overlooked. Looking forward, polarimetry could be a rich new source
794 of information about geospace and could potentially reveal the magnetic structure in the
795 corona and the solar wind in the case of solar radar. Work along these lines is already
796 underway *Salah et al.* [2005]; *Bisi et al.* [2017]; *Lenc et al.* [2017].

797 Wide-band and multi-frequency capabilities represent another new frontier for discovery
798 science. Solar-radar modes are inherently wide band because the modulation schemes
799 involved use frequency-shift keying (FSK).

800 In cases where the target RCS is large enough, e.g., MST, Meteor, FAIs, and perhaps
801 the Moon, coherent and non-coherent MIMO implementations will be useful. The avail-
802 able high power could be diversified to study such targets with unprecedented horizon-
803 tal and altitude resolution and horizontal coverage. For example, FAIs could be studied
804 with simultaneous multi-static links and aperture synthesis radar imaging by employing
805 interferometric configurations on transmission with diversity (e.g., code) and receiving on
806 multiple receiving sites consisting of single antennas (MISO configurations) or more an-
807 tennas (MIMO). This would facilitate studies of FAIs at different scattering points along
808 the Earth's magnetic field in addition to traditional imaging in just the transverse direction.

7. Concluding Remarks

809 A geospace radar as described in this paper would lead not only to a better understanding
810 and practical utilization of the natural echoes studied with existing radars but also to an
811 appreciation of more challenging targets and regions that are waiting to be explored. Here,
812 we have considered just a few research opportunities starting from the lower atmosphere
813 and arriving at the Sun.

814 Although special emphasis has been devoted to applications related to space-weather
815 research and operations like the early detection of the sources of the most extreme events
816 (i.e., CMEs) and efforts to forecast the day-to-day variability of ionospheric irregularities

(e.g., ESF), a geospace radar would contribute to other basic and applied research areas. To name a few: plasma instabilities in the plasmasphere as well as the valley region, turbulence and layering processes in the MST region, meteor composition, meteor mass, solar plasma processes, etc. Furthermore, the receive array portion of the radar could be used passively for radio astronomy or be paired with HF sounders for multistatic ionospheric sounding experiments. **The solar-radar application remains the most compelling single science objective, however, being a compelling new avenue of remote sensing in its own right and holding the promise for end-to-end space-weather forecasting.**

As with any large endeavor, the implementation and subsequent operation of a geospace radar would require a multidisciplinary approach. The effort would necessarily involve, for example, signal processing, statistical inverse theory, software radio, big data handling/processing, machine learning, energy efficient practices, etc. That is, it would require the participation and interaction of a workforce encompassing key disciplines of society drawn from science, technology, engineering, and mathematics (STEM) working toward societal security and prosperity.

Acknowledgments. The Jicamarca Radio Observatory is a facility of the Instituto Geofisíco del Perú operated with support from NSF award AGS-1732209 to Cornell.

References

Bastian, T. S., Progress on the Frequency Agile Solar Radiotelescope, Proc. SPIE 4853, Innovative Telescopes and Instrumentation for Solar Astrophysics, 11 February, 2003.

836 Bastian, T. S., Low-frequency solar radiophysics with LOFAR and FASR, *Planetary and*
837 *Space Science*, *52*, 1381–1389, 2004.

838 Beynon, W. J. G., and P. J. S. Williams, Incoherent scatter of radio waves from the iono-
839 sphere, *Reports on Progress in Phys.*, *41*, 909, 1978.

840 Bisi, M. M., et al., Observations and Analyses of Heliospheric Faraday Rotation of a Coro-
841 nal Mass Ejection (CME) Using the LOw Frequency ARray (LOFAR) and Space-Based
842 Imaging Techniques, in *EGU General Assembly Conference Abstracts*, vol. 19, p. 13243,
843 2017.

844 Chau, J. L., R. F. Woodman, and F. R. Galindo, Sporadic meteor sources as observed by
845 the Jicamarca high-power large-aperture VHF radar, *Icarus*, *188 (1)*, 162–174, 2007.

846 Chau, J. L., R. F. Woodman, M. A. Milla, and E. Kudeki, Naturally enhanced ion-line
847 spectra around the equatorial 150-km region, *Ann. Geophys.*, *27*, 933–942, 2009.

848 Chau, J. L., D. McKay, J. P. Vierinen, C. La Hoz, T. Ulich, M. Lehtinen, and R. Latteck,
849 Multi-static spatial and angular studies of polar mesospheric summer echoes combining
850 maarsy and kaira, *Atmospheric Chemistry and Physics*, *18*, 9547–9560, 2018a.

851 Chau, J. L., J. M. Urco, J. P. Vierinen, R. A. Volz, M. Clahsen, N. Pfeffer, and J. Traut-
852 ner, Novel specular meteor radar systems using coherent mimo techniques to study
853 the mesosphere and lower thermosphere, *Atmospheric Measurement Techniques Dis-*
854 *cussions*, *2018*, 1–23, 2018b.

855 Coles, W. A., Solar radar, in *Solar and Space Weathar Radiophysics*, edited by D. E. Gary
856 and C. Keller, chap. 16, Springer, New York, 2004.

857 Coles, W. A., J. K. Harmon, M. P. Sulzer, J. L. Chau, and R. F. Woodman, An
858 upper bound on the solar radar cross section at 50 MHz, *J. Geophys. Res.*, *111*,
859 doi:10.1029/2005JA011,416, 2006.

860 Cranmer, M. D., et al., Bifrost: A python/c++ framework for high-throughput stream pro-
861 cessing in astronomy, *Journal of Astronomical Instrumentation*, *06*, 1750,007, 2017.

862 Dougherty, J. P., and D. T. Farley, A theory of incoherent scattering of radio waves by a
863 plasma, *Proc. Roy. Soc*, *A259*, 79–99, 1960.

864 Dougherty, J. P., and D. T. Farley, A theory of incoherent scattering of radio waves by a
865 plasma, 3, scattering in a partly ionized gas, *J. Geophys. Res.*, *68*, 5473–5486, 1963.

866 Ellingson, S. W., et al., The LWA1 Radio Telescope, *IEEE Trans. Antennas and Propaga-*
867 *tion*, *5*, 2540–9, 2012.

868 Eshleman, V. R., R. C. Barthle, and P. B. Gallagher, Radar echoes from the Sun, *Science*,
869 *131*, 329–332, 1960.

870 Fallows, R., et al., Broadband meter-wavelength observations of ionospheric scintillation,
871 *Journal of Geophysical Research: Space Physics*, *119*, 10–544, 2014.

872 Farley, D. T., Early incoherent scatter observations at Jicamarca, *J. Atmos. Terr. Phys.*, *53*,
873 665–675, 1991.

874 Farley, D. T., J. P. Dougherty, and D. W. Barron, A theory of incoherent scattering of radio
875 waves by a plasma, 2, Scattering in a magnetic field, *Proc. R. Soc.*, *London Ser. A, 263*,
876 238–258, 1961.

877 Fejer, J. A., Scattering of radio waves by an ionized gas in thermal equilibrium, *Can. J.*
878 *Phys.*, *38*, 1114–1133, 1960.

Fejer, J. A., Scattering of radio waves by an ionized gas in thermal equilibrium in the presence of a uniform magnetic field, *Can. J. Phys.*, pp. 716–740, 1961.

Hagfors, T., Density fluctuations in a plasma in a magnetic field, with applications to the ionosphere, *J. Geophys. Res.*, *66*, 1699–1712, 1961.

Hocking, W., A review of mesospherestratospheretroposphere (mst) radar developments and studies, circa 19972008, *Journal of Atmospheric and Solar-Terrestrial Physics*, *73*, 848 – 882, 2011, scientific Results from Networked and Multi-instrument studies based on MST Radar.

Hysell, D. L., and J. L. Chau, Optimal aperture synthesis radar imaging, *Radio Sci.*, *41*, 10.1029/2005RS003,383, RS2003, 2006.

Hysell, D. L., M. F. Larsen, and M. P. Sulzer, High time and height resolution neutral wind profile measurements across the mesosphere/lower thermosphere region using the Arecibo incoherent scatter radar, *J. Geophys. Res.*, *119*, DOI: 10.1002/2013JA019,621, 2014.

James, J. C., Radar echoes from the Sun, *IEEE Trans. Antennas Propag.*, *AP-12*, 876–891, 1964.

James, J. C., El Campo solar radar data and system design notes, *Tech. Rep. 70-2*, MIT Cent. of Space Res., Cambridge, Mass, 1970.

Kero, A., J. Vierinen, D. McKay-Bukowski, C.-F. Enell, M. Sinor, L. Roininen, and Y. Ogawa, Ionospheric electron density profiles inverted from a spectral riometer measurement, *Geophysical Research Letters*, *41*, 5370–5375, 2014.

Kero, J., C. Szasz, T. Nakamura, D. D. Meisel, M. Ueda, Y. Fujiwara, T. Terasawa, H. Miyamoto, and K. Nishimura, First results from the 20092010 mu radar head echo observation programme for sporadic and shower meteors: the orionids 2009, *Monthly Notices of the Royal Astronomical Society*, *416*, 2550–2559, 2011.

Khotyaintsev, M. V., Theory of solar radar experiments: Combination scattering by anisotropic Langmuir turbulence, Ph.D. thesis, Uppsala University, Uppsala, Sweden, 2005.

Kontar, E. P., S. Yu, A. A. Kuznetsov, A. G. Emslie, B. Alcock, N. L. S. Jeffrey, V. N. Melnik, N. H. Bian, and P. Subramanian, Imaging spectroscopy of solar radio burst fine structures, *Nature Communications*, pp. 1–9, 2017.

Kudeki, E., and M. A. Milla, Incoherent scatter spectral theories–Part I: A general framework and results for small magnetic aspect angles, *IEEE Transactions on Geoscience and Remote Sensing*, *49*, 315–328, 2011.

Lehtinen, M. S., Statistical theory of incoherent scatter radar measurements, *Tech. Rep. 86/45*, Eur. Incoherent Scatter Sci. Assoc., Kiruna, Sweden, 1986.

Lenc, E., et al., The challenges of low-frequency radio polarimetry: Lessons from the Murchison Widefield Array, *Publications of the Astronomical Society of Australia*, *34*, e040, 2017.

Loi, S. T., et al., Real-time imaging of density ducts between the plasmasphere and ionosphere, *J. Geophys. Res.*, *42*, 10.1002/2015GL063,699, 2015.

Maekawa, Y., S. Fukao, M. Yamamoto, M. D. Yamanaka, T. Tsuda, S. Kato, and R. F. Woodman, First observation of the upper stratospheric vertical winds observed by the

922 Jicamarca VHF radar, *Geophys. Res. Lett.*, *20*, 2235, 1993.

923 McCrea, I., et al., The science case for the eiscat_3d radar, *Progress in Earth and Planetary*
924 *Science*, *2*, 21, 2015.

925 McKay-Bukowski, D., et al., Kaira: The kilpisjärvi atmospheric imaging receiver arraysys-
926 tem overview and first results, *IEEE Transactions on Geoscience and Remote Sensing*,
927 *53*, 1440–1451, 2015.

928 Milla, M. A., and E. Kudeki, Incoherent scatter spectral theories–Part II: Modeling the
929 spectrum for modes propagating perpendicular to $\vec{B}$, *IEEE Transactions on Geoscience*
930 *and Remote Sensing*, *49*, 329–345, 2011.

931 Milla, M. A., E. Kudeki, J. L. Chau, and P. M. Reyes, A multi-beam incoherent scatter
932 radar technique for the estimation of ionospheric electron density and t_e/t_i profiles at
933 jicamarca, *Journal of Atmospheric and Solar-Terrestrial Physics*, *105-106*, 214–229,
934 2013.

935 Mondal, S., A. Mohan, D. Oberoi, L. Benkevitch, C. J. Lonsdale, J. Morgan, M. Crowley,
936 and I. Cairns, First results from automated imaging routine for compact arrays for radio
937 sun, *Proceedings of the International Astronomical Union*, *13*, 159–160, 2018.

938 Nicolls, M. J., R. H. Varney, S. L. Vadas, P. A. Stamus, C. J. Heinselman, R. B. Cos-
939 grove, and M. C. Kelley, nfluence of an inertia-gravity wave on mesospheric dynamics:
940 A case study with the Poker Flat Incoherent Scatter Radar, *J. Geophys. Res.*, p. doi:
941 10.1029/2010JD014042, 2010.

942 Oberoi, D., et al., Solar science at metric radio wavelengths: Coming of age, in *IAU Sym-*
943 *posium*, edited by D. Banerjee, J. Jiang, K. Kusano, and S. Solanki, vol. 340 of *IAU*

Symposium, pp. 145–146, 2018.

Oppenheim, M. M., G. Sugar, N. O. Slowey, E. Bass, J. L. Chau, and S. Close, Remote sensing lower thermosphere wind profiles using non-specular meteor echoes, *Geophys. Res. Lett.*, *36*, doi:10.1029/2009GL037,353, 2009.

Parrish, A., Solar radar experiments, 1967, *Tech. rep.*, Center for Radiophysics and Space Physics, Cornell University, 1968.

Perkins, F. W., E. E. Salpeter, and K. O. Yngvesson, Incoherent scatter from plasma oscillations in the ionosphere, *Phys. Rev. Lett.*, *14*, 579–581, 1965.

Rodrigues, P., Radar studies of the solar corona: A review of experiments using HF wavelengths, in *Radio Astronomy at Long Wavelengths*, edited by R. G. Stone, K. W. Weiler, M. L. Goldstein, and J. L. Bougerat, pp. 155–165, American Geophysical Union, 2013.

Rogers, A. E., and J. D. Bowman, Spectral index of the diffuse radio background measured from 100 to 200 mhz, *The Astronomical Journal*, *136*, 641, 2008.

Rosenbluth, M. N., and N. Rostocker, Scattering of electromagnetic waves by a nonequilibrium plasma, *Phys. Fluids*, *5*, 776–788, 1962.

Salah, J. E., C. J. Lonsdale, D. Oberoi, R. J. Cappallo, and J. C. Kasper, Space weather capabilities of low frequency radio arrays, *Proc. SPIE 5901, Solar Physics and Space Weather Instrumentation*, *59010G*, doi: 10.1117/12.613,448, 2005.

Salpeter, E. E., Electron density fluctuations in a plasma, *Phys. Rev.*, *120*, 1528–1535, 1960.

Salpeter, E. E., Plasma density fluctuations in a magnetic field, *Phys. Rev.*, *122*, 1663–1674, 1961.

966 Schult, C., G. Stober, D. Janches, and J. L. Chau, Results of the first continuous meteor
967 head echo survey at polar latitudes, *Icarus*, *297*, 1 – 13, 2017.

968 Sharma, R., D. Oberoi, and M. Arjunwadkar, Quantifying weak nonthermal solar radio
969 emission at low radio frequencies, *The Astrophysical Journal*, *852*, 69, 2018.

970 Stober, G., and J. L. Chau, A multistatic and multifrequency novel approach for specular
971 meteor radars to improve wind measurements in the MLT region, *Radio Science*, *50*,
972 431–442, 2015, 2014RS005591.

973 Stober, G., J. L. Chau, J. Vierinen, C. Jacobi, and S. Wilhelm, Retrieving horizontally
974 resolved wind fields using multi-static meteor radar observations, *Atmospheric Mea-*
975 *surement Techniques Discussions*, *2018*, 1–25, 2018.

976 Taylor, G., Thermospheric neutral wind measurement using the lwa1 and the afrl
977 digisonde, *Tech. rep.*, NEW MEXICO UNIV ALBUQUERQUE DEPT OF PHYSICS
978 AND ASTRONOMY, 2014.

979 Urco, J. M., J. L. Chau, M. A. Milla, J. P. Vierinen, and T. Weber, Coherent mimo to
980 improve aperture synthesis radar imaging of field-aligned irregularities: First results at
981 jicamarca, *IEEE Transactions on Geoscience and Remote Sensing*, *PP*, 1–11, 2018a.

982 Urco, J. M., J. L. Chau, T. Weber, and R. Lateck, Enhancing the spatio-temporal fea-
983 tures of polar mesosphere summer echoes using coherent MIMO and radar imaging at
984 MAARSY, *Atmos. Meas. Tech.*, pp. https://doi.org/10.5194/amt–2018–258, 2018b.

985 van Haarlem, M. P., J. Blo, and J. Otherblo, LOFAR: The low-frequency array, *Astronomy*
986 *and Astrophysics*, *556*, A2, 2013.

Vierinen, J., D. McKay-Bukowski, M. S. Lehtinen, A. Kero, and T. Ulich, Kilpisjärvi atmospheric imaging receiver arrayfirst results, in *Phased Array Systems & Technology, 2013 IEEE International Symposium on*, pp. 664–668, IEEE, 2013.

Vierinen, J., J. L. Chau, N. Pfeffer, M. Clahsen, and G. Stober, Coded continuous wave meteor radar, *Atmospheric Measurement Techniques*, *9*, 829–839, 2016.

Vierinen, J., T. Tveito, B. Gustavsson, S. Kesaraju, and M. Milla, Radar images of the moon at 6-meter wavelength, *Icarus*, *297*, 179–188, 2017.

Virtanen, I., D. McKay-Bukowski, J. Vierinen, A. Aikio, R. Fallows, and L. Roininen, Plasma parameter estimation from multistatic, multibeam incoherent scatter data, *Journal of Geophysical Research: Space Physics*, *119*, 10–528, 2014.

Woodman, R. F., Incoherent scattering of electromagnetic waves by a plasma, Ph.D. thesis, Harvard University, 1967.

Woodman, R. F., and J. L. Chau, Antenna compression using binary phase coding, *Radio Sci.*, *36*, 45, 2001.

Woodman, R. F., and A. Guillén, Radar observations of winds and turbulence in the stratosphere and mesosphere, *J. Atmos. Sci.*, *31*, 493–505, 1974.

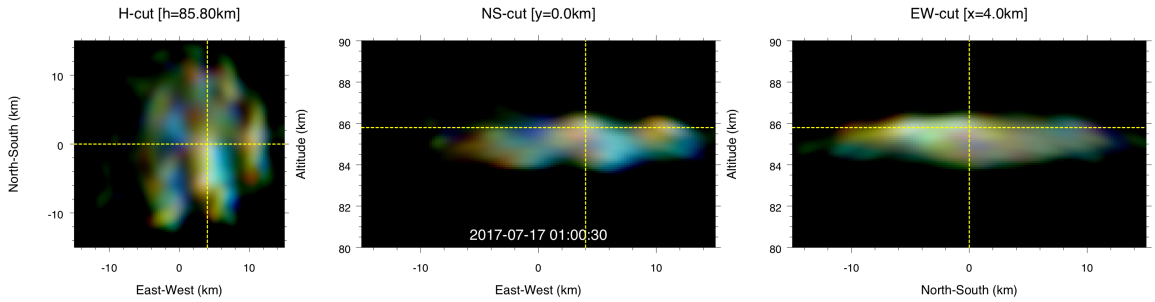

Figure 1. Example of 3D PMSE images obtained with a combination of MaxENT radar imaging and time-diversity MIMO techniques using the MAARSY radar: (a) horizontal cut at 85.80 km, (b) altitude versus zonal cut, and (c) altitude versus meridional cut. Doppler velocity, spectral width, and intensity are color-coded in the images. Adapted from *Urco et al.* [2018b]

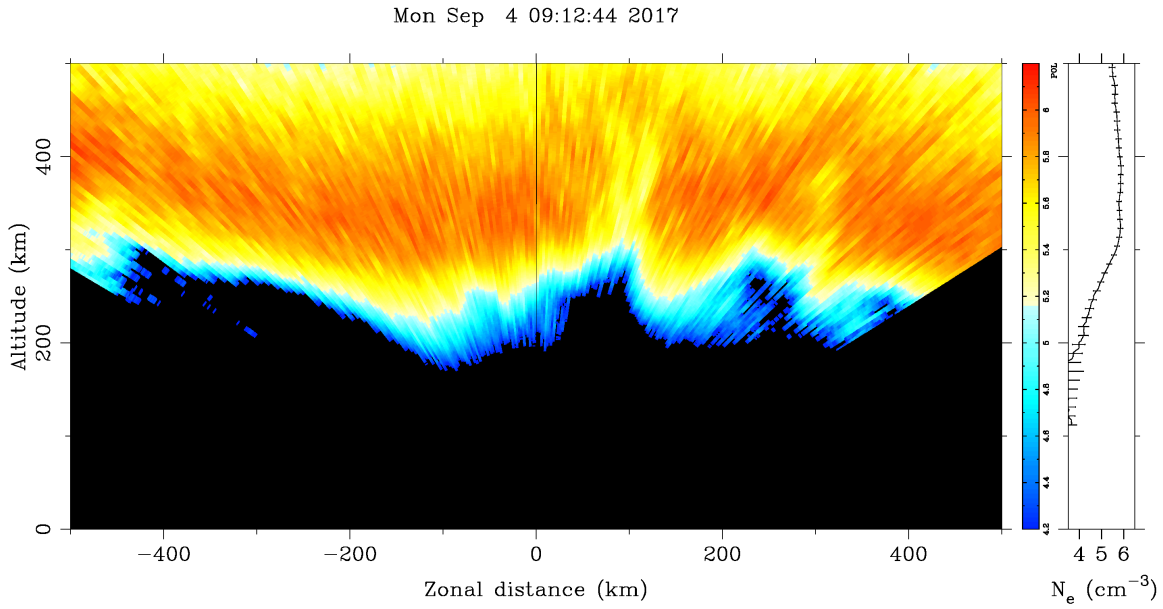

Figure 2. Incoherent scatter observations of large-scale plasma density irregularities and plume-like depletions associated with equatorial spread F made with the ALTAIR radar. The data were acquired with antenna scans directed a few degrees away from perpendicular to the geomagnetic field.

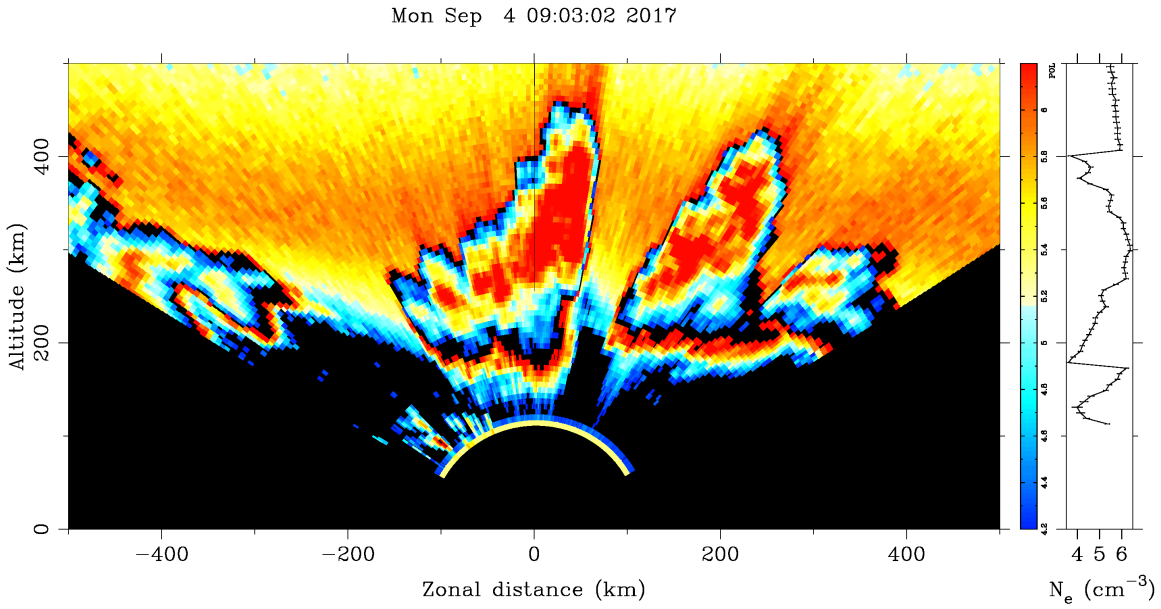

Figure 3. Radar observations of irregularities associated with equatorial spread F made with ALTAIR antenna scans directed perpendicular to the geomagnetic field. Coherent scatter can be observed in the most deeply depleted parts of the F region. In this figure, the coherent scatter is automatically attenuated by 20 dB for plotting.

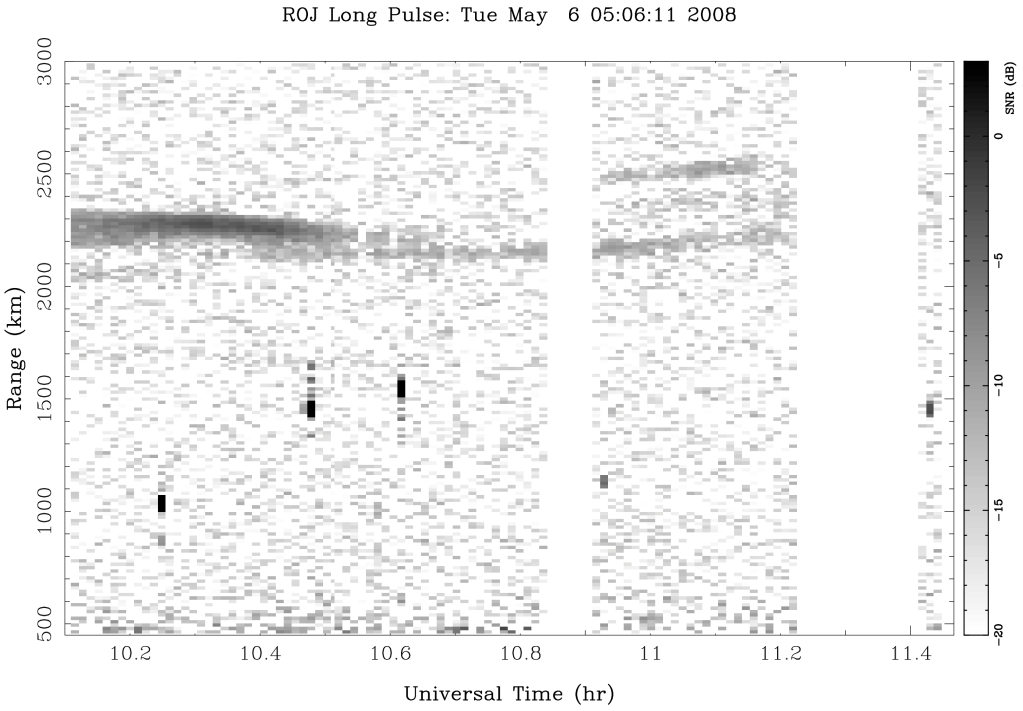

Figure 4. Coherent scatter signal-to-noise ratio derived from topside observations at Jicamarca in the pre-dawn sector. For this figure, radar clutter due to satellites and debris most evident between 1000-1500 km has not been removed.

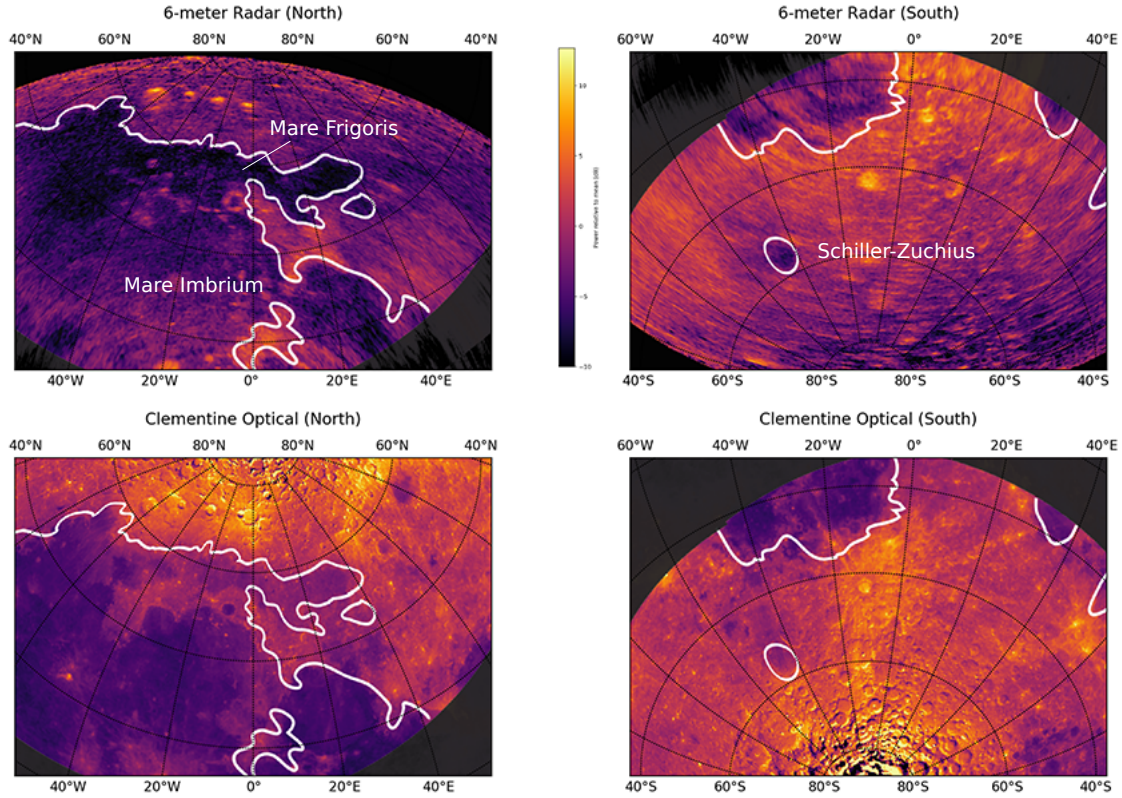

Figure 5. Top: 6-meter wavelength radar map of the Moon derived from Jicamarca data with polarization orthogonal to the specular polarization. Bottom: Clementine optical image of the Moon.

Capability	MST	Meteor	ISR	FAIs	Plasmasphere	Planetary	Solar
High peak power	✓	✓	✓		✓	✓	✓
High duty cycle	✓	✓	✓	✓	✓	✓	✓
Multistatic	✓	✓	✓	✓	✓		✓
Distributed	✓	✓	✓	✓	✓	✓	✓
Polarimetric		✓	✓			✓	✓
Wide band	✓	✓					✓
MIMO	✓	✓		✓			

Table 1. Capabilities versus potential applications.